RSC Advances

PAPER

View Article Online
View Journal | View Issue

Cite this: *RSC Adv.*, 2022, **12**, 12377

Nitrogen self-doped carbon with super high-rate and long cycle life as anode materials for lithium-ion batteries †

Jian Li,[ab] Yanjun Cai, *[ab] Xiang Yao,[ab] Yue Zhang,[c] Hualing Tian[ab] and Zhi Su *[abd]

Nitrogen self-doped carbon was synthesized by hydrothermal and microwave calcination using polyacrylonitrile as a carbon source and nitrogen source. This method dramatically reduces the material preparation time while improving the electrochemical performance of amorphous carbon. X-ray photoelectron spectroscopy (XPS) analyses reveal that the pyridine nitrogen content is increased and the graphitized nitrogen disappeared in an amorphous carbon block. This indicates that the nitrogen doping sites of the amorphous carbon block can be modulated by the hydrothermal method. Microscopic observations show that the nitrogen self-doped carbon is nano-carbon spheres and carbon micron block. The self-doped nitrogen micron carbon block exhibits excellent cyclability and ultra-high rate capacity. When cycled at 0.5 A g^{-1}, the discharge capacity remains 356.6 mA h g^{-1} after 1000 cycles. Even cycled at 5 A g^{-1}, the rate capacity was maintained at 183.3 mA h g^{-1} after 300 cycles. The defects produced by self-doped pyridine nitrogen, not only improved the reactivity and electronic conductivity but also enhanced lithium-ion diffusion kinetics.

Received 10th December 2021
Accepted 8th April 2022

DOI: 10.1039/d1ra08963c

rsc.li/rsc-advances

1 Introduction

Energy and environmental issues are crucial to human development. Traditional non-renewable fossil energy is unsustainable.[1–4] Clean energy such as geothermal energy, tidal energy and solar energy can alleviate the energy crisis.[5–8] However, these energy sources are intermittent.[9–12] To maximize the use of clean energy, the development of and research into energy storage systems has become a decisive factor.[13–15] Among all the alternative energy storage technologies, the lithium-ion battery is widely used in portable electronic devices and electric vehicles due to high power density and energy density, long-term cycling and environmental friendliness.[16,17]

In recent studies, graphite and graphitized carbon materials have been used in commercial lithium-ion batteries due to their low cost, easy synthesis and the abundant raw materials.[18] However, carbon-based anodes have some disadvantages, such as, voltage hysteresis, poor high rate performance and low theoretical capacity.[19] In recent research it has been shown that heteroatom doping, and modification of synthetic methods can solve these problems well.[20] Doping is an effective way to improve material properties.[21] Different heteroatom doping will enhance the surface and internal conformation of carbon.[22] For example, P doping can expand the interlayer distance, promote the migration of lithium ions and electrons, and improve the storage of lithium ions.[21] N doping can make carbon produce external defects, expand the distance between layers, accelerate the diffusion of lithium ions, and improve the electronic conductivity. Li *et al.*[23] proposed a three-dimensional network carbon matrix composite with N and P double doping, which exhibiting excellent cycling performance. A super stable capacity of 195 mA h g^{-1} can be obtained after 1000 cycles at 1 A g^{-1}. Moreover, the essential method is also an important strategy for material modification. Compared with the traditional preparation methods, microblog-assisted technology has the advantages of fast heating speed, uniform heating, short reaction time, high yield, and clean synthesis method. Therefore, it has been widely used in material synthesis.[24,25]

In this study, pyridine nitrogen-rich carbon micro blocks were prepared by microwave carbonization with amidated polyacrylonitrile as a precursor. Nitrogen doping sites can be regulated by hydrothermal reaction. Pyridine nitrogen can produce more defects, provide more active sites, and promote lithium mobility. Self nitrogen-doped micron carbon blocks have ultra-high rate capacity and long-term recyclability.

[a]*College of Chemistry and Chemical Engineering, Xinjiang Normal University, Urumqi, 830054, Xinjiang, China. E-mail: cyjxjsf@yeah.net; suzhixj@sina.com*

[b]*Xinjiang Key Laboratory of Energy Storage and Photoelectrocatalytic Materials, Urumqi, 830054, Xinjiang, China*

[c]*State Key Laboratory of Chemistry and Utilization of Carbon Based Energy Resources, Key Laboratory of Advanced Functional Materials, Autonomous Region, Institute of Applied Chemistry, College of Chemistry, Xinjiang University, Urumqi, 830046, Xinjiang, PR China*

[d]*Xinjiang Institute of Technology, China*

† Electronic supplementary information (ESI) available. See https://doi.org/10.1039/d1ra08963c

2 Experimental

2.1 Synthesis of materials

The reagent used in the experiment is polyacrylonitrile (PAN, molecular weight 250 000, Dongguan Huachuang Plastics Co., Ltd) and ammonia water (Tianjin Xinbote Chemical Co., Ltd). All reagents were directly used without further pretreatment. The PAN (1 g) was mixed with ammonia water (1 mL, 3 mL, 5 mL, 7 mL, 9 mL, 11 mL, 13 mL) in different proportions, stirred at 25 °C for 30 min. A clear yellow solution was obtained by hydrothermal reaction at 180 °C for 12 h. The yellow clarification solution was dried 140 °C for 12 h and then ground to obtain a light yellow powder. The prepared precursors were denoted as HPAN-1:1, HPAN-1:3, HPAN-1:5, HPAN-1:7, HPAN-1:9, HPAN-1:11 and HPAN-1:13. The precursors were calcined in a microwave oven at optimal power of 750 W and optimal time of 15 min to obtain nano-carbon and carbon micron blocks, denoted as HPC-1:1, HPC-1:3, HPC-1:5, HPC-1:7, HPC-1:9, HPC-1:11 and HPC-1:13. For comparison, PC was obtained by direct microwave calcination of polyacrylonitrile at the above optimal power and time.

2.2 Characterization of materials

X-ray diffraction (XRD) of the as-prepared samples was tested by a Bruker D2 system (Cu Kα radiation, $\lambda = 1.5418$, step size: 0.02°). The degrees of graphitization of as-prepared samples were measured using confocal Raman spectroscopy under laser excitation at 532 nm. Fourier transform infrared was conducted by a Bruker Tensor 27 FTIR spectrometer. High-resolution transmission electron microscopy (HRTEM, ZEISS Libra 200 FE) was used to study the microstructure of nano-carbon and carbon blocks. X-ray photoelectron spectroscopy (XPS, Thermo Fischer, ESCALAB Xi+, America) was used to measure the distribution of elements, the valence state, in the vacuum chamber with a vacuum degree of 8×10^{-10} Pa.

2.3 Electrochemical performance tests

The coin-type cell (2032) was assembled used to test electrochemical performance. To prepare the working electrode, the synthesized sample, acetylene black and polyvinylidene fluoride were mixed at a mass ratio of 8 : 1 : 1. Then stir to form a slurry in *N*-methyl-pyrrolidone. The slurry was spread on the copper foil and then dried in a vacuum at 110 °C for 12 hours. Cut it into a disc as working electrode with a diameter of 10 mm. The counter electrode is lithium metal. Celgard 2400 serves as a diaphragm. The electrolyte was formed by dissolving 1 M $LiPF_6$ in a mixture of vinyl carbonate (EC), dimethyl carbonate (DMC), methyl ethyl carbonate (EMC) with a volume ratio of 1 : 1 : 1. In a glove box filled with argon gas (water and oxygen content is less than <0.01 ppm), the cells are assembled in the order of negative shell, lithium metal, diaphragm, work electrode, gasket, shrapnel, and positive shell. The cycle performance was tested by the CT2001A system between 0.01–3 V. Cyclic voltammetry (CV) was performed on the electrochemical workstation (CHI760E, 0.01–3 V, 0.1 mV s^{-1}). The electrochemical workstation was used to test the AC impedance at the frequency of 10^{-1} to 10^{5} Hz and the amplitude of 5 mV.

3 Results and discussion

Fig. 1(a) shows the different types of nitrogen doping configurations. N-5, N-6 and N-Q represent pyrrole nitrogen and pyridine nitrogen, graphitized nitrogen, respectively. The hydrolysis mechanism of the reaction is shown in Fig. 1(b). Firstly, the nucleophilic addition reaction occurs when OH^- attacks the carbon atom in –C≡N in an alkaline solution. In this process, –C≡N breaks, and OH^- forms a covalent bond with the carbon atom. The negative charge is transferred to the nitrogen atom, resulting in the electronegative intermediate B. Because of its strong nucleophilic ability, some intermediates continue to undergo a nucleophilic addition reaction with adjacent cyano groups to form a hexagonal ring structure. Meanwhile, the negative charge is still transferred to the cyano nitrogen atom to be added. The negative charge nitrogen atom reacts with adjacent cyano groups to form a series of hexagonal rings with covalent bonds. See the molecular formula C. Substance C reacts with water to form amide, which is hydrolyzed under alkaline conditions to form carboxylic acid E. Another possible mechanism is that intermediate B can combine with water and undergo reciprocal isomerization to produce amide. See molecular formula F and G. Amides are attacked by OH^- in an alkaline environment and eventually hydrolyzed to form carboxylic acids. As shown in Fig. 1(c), amidated polyacrylonitrile was obtained by hydrolyzing polyacrylonitrile with ammonia, dried and microwave carbonized to obtain HPC.

As shown in Fig. 2(a) and S1,† the structure of nano-carbon and micron carbon blocks synthesized under different conditions was tested by XRD. The XRD patterns of all samples show two broad peaks at 25.5° and 42.7°, which is consistent with the standard card PDF#26-1077. It can be concluded that pure phase carbon was synthesized under all conditions.[26] From Fig. 2(a), it can be observed that the XRD patterns of the HPC-1:13 peak slightly decreases compared to HPC-1:11 or other samples. This phenomenon can be attributed to the increase of ammonia concentration, which leads to the increase of nitrogen doping content in the material compared with other samples.[27] With the increase of nitrogen doping, the intensity of

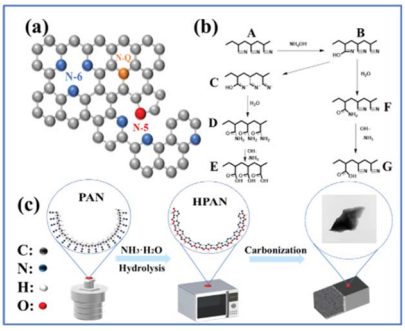

Fig. 1 (a) Nitrogen doped configuration, (b) hydrolysis reaction mechanism diagram, (c) synthesis path of HPC.

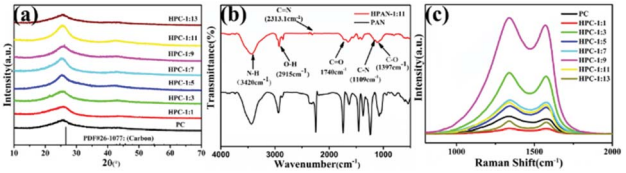

Fig. 2 (a) XRD patterns of PC and a series of HPC, (b) infrared spectra of PAN and HPAN-1:11, (c) Raman spectra of PC and a series of HPC.

diffraction peak (HPC-1:11) decreases significantly, indicating that high-dose nitrogen doping will reduce the structural ordering of carbon.[28] To explore the chemical bonding of precursors, the infrared spectra of PAN and HPAN-1:11 are studied. As shown in Fig. 2(b), compared with PAN, the appearance of C=O at 1740 cm^{-1} and C–O at 1397 cm^{-1} in HPAN-1:11 may be caused by the nucleophilic addition reaction between PAN and $NH_3 \cdot H_2O$ to form carboxyl group. In HPAN-1:11, the nitrile group peak decreased significantly at 2313 cm^{-1} and the internal peak was missing from 805 cm^{-1} to 1836 cm^{-1}. It supported the absence of nitrogen-containing functional groups in the reaction mechanism.[29] For further study of the structural and electronic properties of nitrogen self-doped carbon, Raman spectra were measured. As shown in Fig. 2(c), all samples have two bands corresponding to the wide D-band and G-band at 1345–1340 cm^{-1} and 1572–1585 cm^{-1}, respectively. D-band and G-band were caused by defects in the graphite structure and the ideal.[30] The relative strength of the D and G bands can reflect the degree of carbon graphitization and defect.[31] Nitrogen self-doped carbon synthesized with different ammonia concentrations of 0 mL, 1 mL, 3 mL, 5 mL, 7 mL, 9 mL, 11 mL and 13 mL, the values of I_D/I_G were 0.96, 0.95, 0.97, 0.96, 0.96, 0.99, 0.99 and 1.00, respectively. With the increase in ammonia concentration, the degree of defects in carbon materials also increases.[28]

The internal structures of nitrogen self-doped carbon are characterized by TEM. Fig. 3(a) and (b) are TEM of PC and HPC-1:11, respectively. The morphology shows that PC is a carbon nano-sphere and HPC-1:11 is a carbon micro block. With increasing ammonia concentration, the synthesized materials transform from nanoparticles to micron blocks and subsequently to nanoparticles, see Fig. S2.† When the ammonia content was 11 mL, the morphology of the nanocarbon was changed as a micron carbon block. This can be attributed to the hydrophobicity of graphitized nitrogen in the presence of ammonia. When graphitized nitrogen disappears, it will lead to the aggregation of nanoparticles. With the increase of ammonia concentration, a similar evolution of nitrogen self-doping carbon morphology was also observed by scanning electron microscopy (Fig. S3†). As shown in Fig. 3(c) and (d), the microstructures of PC and HPC-1:11 were characterized by HRTEM, which revealed a highly disordered structure of amorphous carbon. Several graphitic local structures are present in PC with a distinct turbo-layered carbon structure (as shown in the area selected).[32] The disappearance of local graphitic structures in HPC-1:11 is evidence of an increase in disordered carbon.[33] In addition, Fig S4† shows the obtained EDX mapping images of the C, N and O elements of HPC-1:11. The uniform distribution of N is further evidence that N has been doped into HPC-1:11.[34]

The elemental composition and functional group structure of nitrogen self-doped carbon were analyzed by XPS. As shown in Fig. S5(a) and (b),† the XPS spectra of PC and HPC-1:11 show three different peaks: C1s, N1s and O1s, which are observed at 286.1 eV, 401.7 eV, 534.2 eV, and 283.7 eV, 399.2 eV, 532.1 eV, respectively. As shown in Fig. 4(a), the C1s peaks of PC can be divided into four peaks at 284.7 eV, 285.9 eV, 287.1 eV and 289.1 eV, respectively, corresponding to the C–C, C–O–C, C=O and O=C–O. In Fig. 4(b), the C1s peaks of HPC can be divided into five peaks at 284.8 eV, 285.8 eV, 287.1 eV, 289.1 eV and 290.1 eV, respectively, corresponding to the C–C, C–O–C, C=O, O=C–O and C–O. Compared with PC, the additional C–O in HPC-1:11 may be caused by the nucleophilic addition reaction during hydrolysis. It is consistent with the mechanism analysis. In Fig. 4(c), the N1s peaks of PC are located at 398.5 eV, 400.1 eV, 401.2 eV, 404.0 eV, which correspond to pyridine-type N, pyrrole-type N, graphitized-type N, and NO_x. In Fig. 4(d), the N1s peaks of HPC-1:11 located at 398.5 eV, 400.4 eV correspond to

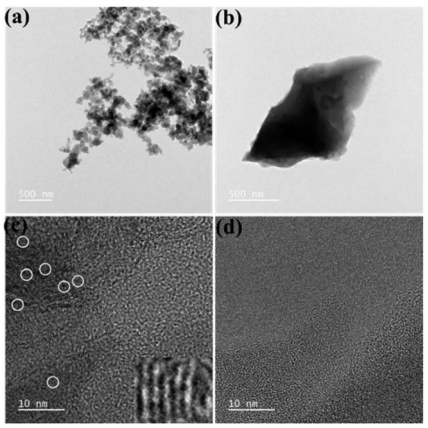

Fig. 3 TEM of (a) PC, (b) HPC-1:11; HRTEM images of (c) PC, (d) HPC-1:11.

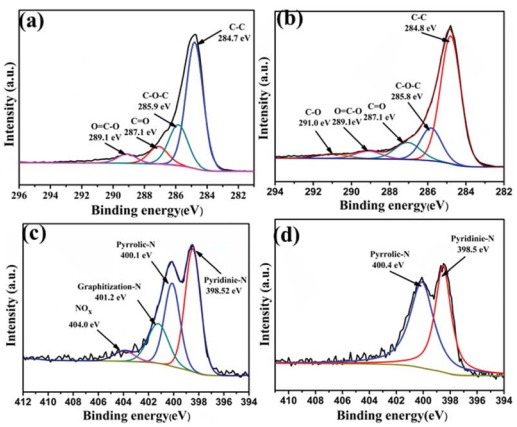

Fig. 4 C1s peak of (a) PC and (b) HPC, N1s peak of (c) PC and (d) HPC-1:11.

pyrrole-type N and pyridine type N. Compared to PC, the graphitized N and NO_x are disappeared in HPC-1:11, as shown in Table S1.† It is favourable evidence to further support the absence of nitrogen-containing functional groups in the reaction mechanism. This phenomenon demonstrated that the type of doped nitrogen in amorphous carbon could be regulated by hydrothermal reaction.[35]

Compared to graphitized nitrogen (N-Q), pyridine nitrogen (N-6) substitute carbon atom at the edge of defect or graphite plane with nitrogen atom, which makes it easier to obtain electrons.[36] Furthermore, pyridine nitrogen can produce more defects and a large number of active centers, which is considered to be the most effective coordination nitrogen to improve the electrode capacity[37,38]

The long cyclability of as-prepared samples at 1 A g^{-1} as shown in Fig. 5(a). It can be observed that irreversible capacity loss occurred in all samples at the initial cycle, due to solid electrolyte (SEI) film being formed.[27] From the second cycle, it shows stable capacity decay. The discharge capacity of HPC-1:11 is significantly higher than that of other nano-carbon materials, which exhibit the best cycle performance (in addition, calcination time and power are explored as shown in Fig. S6†). It can be concluded that optimizing of the ratio of polyacrylonitrile and ammonia, calcination time and calcination power can significantly improve the capacity. Fig. 5(b) shows the 1–3rd charge and discharge curves of HPC-1:11 at 1 A g^{-1}. The charge capacity is 259.7 mA h g^{-1}, the discharge capacity is 682.2 mA h g^{-1} and the coulomb efficiency is 38.1% at the initial cycle. The low coulomb efficiency for the as-prepared sample of HPC-1:11 can be attributed to the electrolyte–electrode activation at high rates (1000 mA g^{-1}) and solid electrolyte membrane formed in the interface.[33] From the 2–3rd cycle, the charge and discharge curves overlap well. Fig. 5(c) shows the 1–3rd CV curves of nitrogen self-doped carbon between voltage range of 0.01–3 V at a scanning rate of 0.1 mV s^{-1}. In first CV curve of HPC-1:11 shows three reduction peaks at 1.8 V, 0.8–1.0 V, and 0.01 V, respectively. The peaks at 1.8 V and 0.8–1.0 V may be due to the decomposition of the solid electrolyte and the formation of SEI.[39] Neither of these above peaks appeared in the second and third CV curves, indicating that the reaction is irreversible. The peak at 0.01 V may be caused by the insertion of lithium ions into the nitrogen self-doped carbon.[40] In the second cycle, the peaks at 0.01 V are appeared again, indicating that the insertion of lithium ions is reversible, which is similar to the recent report.[41] The rate performance of HPC-1:11 was tested, as shown in Fig. 5(d). The charge and discharge rate capacities were maintained at 484.7/488.4 mA h g^{-1}(0.5 A g^{-1}), 275.2/272.6 mA h g^{-1} (1 A g^{-1}), 248.2/249.2 mA h g^{-1} (2 A g^{-1}), and 183.3/187.5 mA h g^{-1} (5 A g^{-1}) after 300 cycles. In Fig. 5(e), the charge and discharge specific capacity of HPC-1:11 can maintain at 356.9/356.6 mA h g^{-1} (0.5 A g^{-1}) and 249.2/256.3 mA h g^{-1} (1 A g^{-1}) after 1000 cycles, which showing long lifespan cycle performance. The excellent cyclability and super high-rate performance of nitrogen self-doped carbon (HPC-1:11) are better than the previously reported lithium-ion anode carbonaceous materials,[30,36,41,44–50] as shown in Table 1.

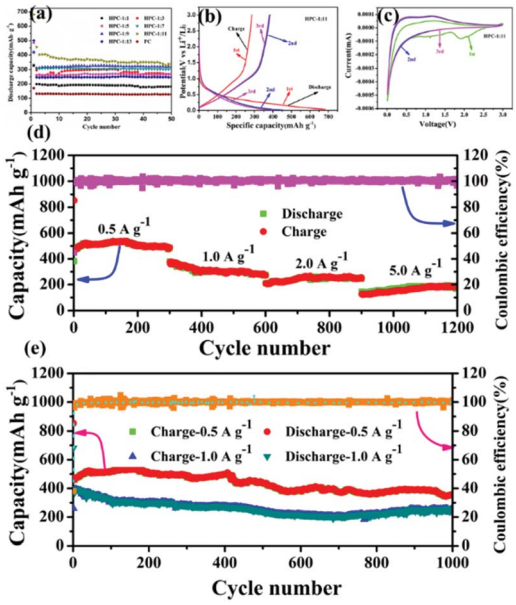

Fig. 5 (a) Cycle performance of PC and a series of HPC; the HPC-1:11 of (b) discharge/charge voltage curves, (c) CV curves (d) rate performance (e) cycle performance at 0.5 A g^{-1} and 1.0 A g^{-1}.

Nitrogen self-doped carbon exhibits super high-rate capacity (higher than the theoretical capacity of graphite) and long-term cyclability. It can be ascribed to the following reasons: firstly, nitrogen doping sites of amorphous carbon can be modulated by the hydrothermal method, which can provide an additional active site and defects for lithium storage. Secondly, nitrogen self-doped can effectively facilitate electron transfer and improve electronic conductivity. Furthermore, pyridine nitrogen has more incredible formation energy, there for a more stable structure could be formed, which facilitates the insertion and extraction of lithium ions.[49,50]

To further explore the reasons for the excellent electrochemical performance of HPC-1:11, AC impedance tests were performed on PC and HPC-1:11. The results are shown in Fig. 6(a). The semicircle diameter at high frequency is related to the charge transfer resistance (R_{ct}) at the interface between electrode material and electrolyte, and the slope of the straight line at low frequency represents the diffusion rate of lithium ions.[51] The kinetic parameters fitted by the equivalent circuit diagram are shown in Fig. 6(b) and Table S2.† The parameters used in this model are R_s (contact resistance), R_{ct}, CPE (constant phase element) and W_o (Warburg impedance).[52] The charge transfer impedance of HPC-1:11 (152.0 Ω) is smaller than that of PC (176.0 Ω), which indicates that HPC-1:11 has high electronic conductivity. Compared with PC ($W_o - R$ is 102.0 Ω), the $W_o - R$ of HPC-1:11 (100.0 Ω) is reduced, which demonstrates that the lithium-ion diffusion rate is faster.[53]

In addition, the kinetic properties of the lithium ion diffusion process are analyzed by eqn (1) and (2) to derive the migration rate of lithium ions in nano-carbon and carbon micron blocks.

$$Z = R_s + R_{ct} + \delta\omega^{-1/2} \quad (1)$$

Table 1 Cycle performance of nitrogen doped carbon

Materials	Current density	Specific capacity	References
N-doped porous carbon	3.72 A g^{-1}	116 mA h g^{-1}	42
Carbon nanomaterials	0.74 A g^{-1}	190 mA h g^{-1}	43
N-doped carbon microspheres	0.50 A g^{-1}	465 mA h g^{-1}	44
Carbon nanotubes	1.00 A g^{-1}	412 mA h g^{-1}	45
N-doped carbon microspheres	1.00 A g^{-1}	292 mA h g^{-1}	41
N-doped ordered mesoporous carbons	1.00 A g^{-1}	~150 mA h g^{-1} ~400 mA h g^{-1}	28
Nitrogen-doped porous carbon microspheres	0.10 A g^{-1} 0.50 A g^{-1}	443 mA h g^{-1} 377 mA h g^{-1}	37
Nitrogen-doped nano-carbon	0.10 A g^{-1}	160 mA h g^{-1}	46
Hollow carbon nanospheres	0.74 A g^{-1}	337 mA h g^{-1}	47
Carbon nanospheres	0.74 A g^{-1}	~350 mA h g^{-1}	48
Nitrogen doped carbon nanoparticles	0.50 A g^{-1} 1.00 A g^{-1} 5.00 A g^{-1}	485 mA h g^{-1} 363 mA h g^{-1} 183 mA h g^{-1}	This work

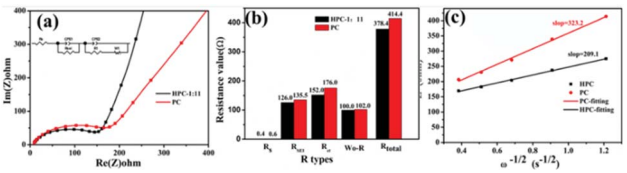

Fig. 6 (a) AC impedance diagram and fitting diagram of PC and HPC-1:11 (b) histogram of impedance fitting data (c) plot of Z' *versus* $\omega^{-1/2}$.

$$D = R^2T^2/2n^4\delta^2C^2A^2F^4 \quad (2)$$

The symbols in the equation represent the following meanings: D (lithium ions diffusion coefficient), R (gas constant), T (absolute temperature), A (surface area of electrode), n (electron transfer number), δ (warburg factor), C (lithium ions concentration), and F (Faraday constant).[54] As shown in Fig. 6(c), D (1.31×10^{-14} cm^2 s^{-1}) of the HPC-1:11 electrode is more than that of the PC electrode (5.50×10^{-15} cm^2 s^{-1}), indicating that HPC-1:11 can provide faster kinetic performance. Warburg impedance of HPC-1:11 is inclined more than 45° compared PC sample. Indeed, the Li-ion diffusion of HPC-1:11 should be lower because the resistance component is dominant. However, the HPC-1:11 may have good capacitance characteristics and therefore good dynamic performance. In addition, after the CV and GITT tests of the sample and calculation of its lithium-ion diffusion coefficient, it is further proved that HPC-1:11 has better kinetic performance (see the Fig. S7† for details).

4 Conclusions

Nitrogen self-doped carbon rich in pyridine nitrogen was prepared from polyacrylonitrile by microwave carbonization alkali hydrolysis. Nitrogen doping sites of amorphous carbon can be modulated by the hydrothermal method, which increases the content of pyridine nitrogen. The nitrogen self-doped micron carbon block showed excellent electrochemical performance as an anode for lithium batteries. At 0.5 A g^{-1} and 1.0 A g^{-1}, after 1000 cycles, the charge–discharge specific capacity can still reach 356.9/356.6 mA h g^{-1} and 249.2/256.3 mA h g^{-1}. Even cycled at 5 A g^{-1}, the rates capacity can reach 187.5 mA h g^{-1}. Nitrogen self doping not only provides additional active centers and defects for lithium storage but also effectively promotes electron transfer and improves electron conductivity. This strategy of regulating nitrogen doping sites by hydrothermal method provides references for nitrogen doping carbon modification methods.

Conflicts of interest

There are no conflicts to declare.

Acknowledgements

This study was supported by Foundation of State Key Laboratory of Chemistry and Utilization of Carbon-based Energy Resource (Grant No. KFKT2021005), Xinjiang Key research and development project in China (2021B01001-1), the National Natural Science Foundation of China (22169020), Dr Tianchi of the "Hundred Young Doctors Introduction Program" of the Autonomous Region (BS2017003).

References

1 Y.-G. Lee, S. Fujiki, C. Jung, N. Suzuki, N. Yashiro, R. Omoda, D.-S. Ko, T. Shiratsuchi, T. Sugimoto, S. Ryu, J. H. Ku, T. Watanabe, Y. Park, Y. Aihara, D. Im and I. T. Han, *Nat. Energy*, 2020, **5**, 299–308.
2 X. Liu, L. Yin, D. Ren, L. Wang, Y. Ren, W. Xu, S. Lapidus, H. Wang, X. He, Z. Chen, G.-L. Xu, M. Ouyang and K. Amine, *Nat. Commun.*, 2021, **12**, 1–11.
3 W. Zuo, X. Liu, J. Qiu, D. Zhang, Z. Xiao, J. Xie, F. Ren, J. Wang, Y. Li, G. F. Ortiz, W. Wen, S. Wu, M.-S. Wang, R. Fu and Y. Yang, *Nat. Commun.*, 2021, **12**, 1–11.
4 J. Yang, Y. Zhai, X. Zhang, E. Zhang, H. Wang, X. Liu, F. Xu and S. Kaskel, *Adv. Energy Mater.*, 2021, **11**, 1–11.
5 L. Xie, C. Tang, Z. Bi, M. Song, Y. Fan, C. Yan, X. Li, F. Su, Q. Zhang and C. Chen, *Adv. Energy Mater.*, 2021, **11**, 1–22.

6 P. Liu, Y. Li, Y.-S. Hu, H. Li, L. Chen and X. Huang, *J. Mater. Chem. A*, 2016, **4**, 13046–13052.
7 B. Huang, X. Li, Y. Pei, S. Li, X. Cao, R. C. Massé and G. Cao, *Small*, 2016, **12**, 1945–1955.
8 L. Zhang, W. Wang, S. Lu and Y. Xiang, *Adv. Energy Mater.*, 2021, **11**, 1–15.
9 H. Liu, X. Liu, W. Li, X. Guo, Y. Wang, G. Wang and D. Zhao, *Adv. Energy Mater.*, 2017, **7**, 1–24.
10 F. Zhang, X. Yang, Y. Xie, N. Yi, Y. Huang and Y. Chen, *Carbon*, 2015, **82**, 161–167.
11 P. Jing, Q. Wang, B. Wang, X. Gao, Y. Zhang and H. Wu, *Carbon*, 2020, **159**, 366–377.
12 F. Sun, H. Wang, Z. Qu, K. Wang, L. Wang, J. Gao, J. Gao, S. Liu and Y. Lu, *Adv. Energy Mater.*, 2020, **11**, 1–13.
13 R. Mo, X. Tan, F. Li, R. Tao, J. Xu, D. Kong, Z. Wang, B. Xu, X. Wang, C. Wang, J. Li, Y. Peng and Y. Lu, *Nat. Commun.*, 2020, **11**, 1–11.
14 Y.-T. Weng, H.-W. Liu, A. Pei, F. Shi, H. Wang, C.-Y. Lin, S.-S. Huang, L.-Y. Su, J.-P. Hsu, C.-C. Fang, Y. Cui and N.-L. Wu, *Nat. Commun.*, 2019, **10**, 1–10.
15 C. Li, X. Zhang, K. Wang, X. Sun, Y. Xu, F. Su, C.-M. Chen, F. Liu, Z.-S. Wu and Y. Ma, *NPG Asia Mater.*, 2021, **13**, 2–16.
16 Y. Tang, X. Wang, J. Chen, X. Wang, D. Wang and Z. Mao, *Carbon*, 2021, **174**, 98–109.
17 H. Hou, X. Qiu, W. Wei, Y. Zhang and X. Ji, *Adv. Energy Mater.*, 2017, **7**, 1–30.
18 B. H. Hou, Y. Y. Wang, Q. L. Ning, W. H. Li, X. T. Xi, X. Yang, H. J. Liang, X. Feng and X. L. Wu, *Adv. Mater.*, 2019, **31**, 1–8.
19 H. Zhang, J. Yang, H. Hou, S. Chen and H. Yao, *Sci. Rep.*, 2017, **7**, 1–9.
20 S.-H. Lee, M. Kotal, J.-H. Oh, P. Sennu, S.-H. Park, Y.-S. Lee and I.-K. Oh, *Carbon*, 2017, **119**, 355–364.
21 W. Chen, M. Wan, Q. Liu, X. Xiong, F. Yu and Y. Huang, *Small Methods*, 2018, **3**, 1–18.
22 J. Wu, Z. Pan, Y. Zhang, B. Wang and H. Peng, *J. Mater. Chem. A*, 2018, **6**, 12932–12944.
23 C. Li, Q. Fu, K. Zhao, Y. Wang, H. Tang, H. Li, H. Jiang and L. Chen, *Carbon*, 2018, **139**, 1117–1125.
24 X. Hou, Y. Li and C. Zhao, *Aust. J. Chem.*, 2016, **69**, 357–361.
25 B. Zheng, Y. Chen, P. Li, Z. Wang, B. Cao, F. Qi, J. Liu, Z. Qiu and W. Zhang, *Nanophotonics*, 2017, **6**, 259–267.
26 Z. Wang, K. Dong, D. Wang, F. Chen, S. Luo, Y. Liu, C. He, C. Shi and N. Zhao, *Chem. Eng. J.*, 2019, **371**, 356–365.
27 W. Zhao, X. Hu, S. Ci, J. Chen, G. Wang, Q. Xu and Z. Wen, *Small*, 2019, **15**, 1–9.
28 G. Wu, C. Shao, S. Qiu, H. Chu, Y. Zou, C. Xiang, H. Zhang, F. Xu and L. Sun, *ChemistrySelect*, 2017, **2**, 10076–10081.
29 Q. Zhao, W. Xiao, X. Yan, S. Qin, B. Qu and L. Zhao, *Ionics*, 2017, **23**, 1685–1692.
30 F. Yang, Z. Zhang, K. Du, X. Zhao, W. Chen, Y. Lai and J. Li, *Carbon*, 2015, **91**, 88–95.
31 K. Yu, Y. Wang, X. Wang, W. Liu, J. Liang and C. Liang, *Mater. Lett.*, 2019, **253**, 405–408.
32 P. Lu, Y. Sun, H. Xiang, X. Liang and Y. Yu, *Adv. Energy Mater.*, 2018, **8**, 1–8.
33 W. Guo, X. Li, J. Xu, H. K. Liu, J. Ma and S. X. Dou, *Electrochim. Acta*, 2016, **188**, 414–420.
34 Y. Cai, Y. Huang, W. Jia, Y. Zhang, X. Wang, Y. Guo, D. Jia, W. Pang, Z. Guo and L. Wang, *J. Mater. Chem. A*, 2016, **4**, 17782–17790.
35 B. Zhao, Y. Ding and Z. Wen, *Trans. Tianjin Univ.*, 2019, **25**, 429–436.
36 Y. Xie, Y. Chen, L. Liu, P. Tao, M. Fan, N. Xu, X. Shen and C. Yan, *Adv. Mater.*, 2017, **29**, 1–9.
37 Y. Gao, X. Qiu, X. Wang, X. Chen, A. Gu and Z. Yu, *Nanotechnology*, 2020, **31**, 1–20.
38 Y. Sun, Y. Zhang, Z. Xing, D. Wei, Z. Ju and Q. Zhuang, *Sustain. Energy Fuels*, 2020, **4**, 1216–1224.
39 Q. Feng, H. Li, Z. Tan, Z. Huang, L. Jiang, H. Zhou, H. Pan, Q. Zhou, S. Ma and Y. Kuang, *J. Mater. Chem. A*, 2018, **6**, 1–22.
40 Y. Tang, X. Wang, J. Chen, X. Wang, D. Wang and Z. Mao, *Carbon*, 2020, **168**, 458–467.
41 H. Hou, C. Yu, X. Liu, Y. Yao, Z. Dai and D. Li, *J. Mater. Cycles Waste Manag.*, 2019, **21**, 1123–1131.
42 A. Gomez-Martin, J. Martinez-Fernandez, M. Ruttert, M. Winter, T. Placke and J. Ramirez-Rico, *Carbon*, 2020, **164**, 261–271.
43 R. Kali, B. Padya, T. N. Rao and P. K. Jain, *Diamond Relat. Mater.*, 2019, **98**, 1–6.
44 D. Sun, X. Yan, J. Yang, P. Zhang and Q. Xue, *Chemelectrochem*, 2015, **2**, 1830–1838.
45 M. Wu, J. Chen, C. Wang, F. Wang and B. Yi, *Electrochim. Acta*, 2013, **105**, 462–467.
46 K. Shi, J. Liu and R. Chen, *J. Energy Storage*, 2020, **31**, 1–6.
47 F.-D. Han, Y.-J. Bai, R. Liu, B. Yao, Y.-X. Qi, N. Lun and J.-X. Zhang, *Adv. Energy Mater.*, 2011, **1**, 798–801.
48 K. Yu, J. Wang, K. Song, X. Wang, C. Liang and Y. Dou, *Nanomaterials*, 2019, **9**, 1–13.
49 Y. Fujimoto and S. Saito, *Phys. E*, 2011, **43**, 677–680.
50 Y. Shang, J.-x. Zhao, H. Wu, Q.-h. Cai, X.-g. Wang and X.-z. Wang, *Theor. Chem. Acc.*, 2010, **127**, 727–733.
51 G. B. Berhe, W.-N. Su, C.-J. Huang, T. M. Hagos, T. T. Hagos, H. K. Bezabh, M. A. Weret, L. H. Abrha, Y.-W. Yang and B.-J. Hwang, *J. Power Sources*, 2019, **434**, 1–9.
52 G. B. Berhe, W.-N. Su, L. H. Abrha, H. K. Bezabh, T. M. Hagos, T. T. Hagos, C.-J. Huang, N. A. Sahalie, B. A. Jote, B. Thirumalraj, D. Kurniawan, C.-H. Wang and B. J. Hwang, *J. Mater. Chem. A*, 2020, **8**, 14043–14053.
53 Y. Chao, Y. Ge, Y. Zhao, J. Jiang, C. Wang, C. Qin, A. Vijayakumar, C. Yu and G. G. Wallace, *Electrochim. Acta*, 2018, **291**, 197–205.
54 B. Kurc and M. Pigłowska, *J. Power Sources*, 2021, **485**, 229323–229332.